Journal of Materials Chemistry A

PAPER

View Article Online
View Journal | View Issue

Cite this: J. Mater. Chem. A, 2015, 3, 22432

Benchmarking density functional theory predictions of framework structures and properties in a chemically diverse test set of metal–organic frameworks†

Dalar Nazarian,[a] P. Ganesh[b] and David S. Sholl*[a]

Received 28th May 2015
Accepted 23rd September 2015

DOI: 10.1039/c5ta03864b

www.rsc.org/MaterialsA

A test set of chemically and topologically diverse Metal–Organic Frameworks (MOFs) with high accuracy experimentally derived crystallographic structure data was compiled. The test set was used to benchmark the performance of Density Functional Theory (DFT) functionals (M06L, PBE, PW91, PBE-D2, PBE-D3, and vdW-DF2) for predicting lattice parameters, unit cell volume, bonded parameters and pore descriptors. On average PBE-D2, PBE-D3, and vdW-DF2 predict more accurate structures, but all functionals predicted pore diameters within 0.5 Å of the experimental diameter for every MOF in the test set. The test set was also used to assess the variance in performance of DFT functionals for elastic properties and atomic partial charges. The DFT predicted elastic properties such as minimum shear modulus and Young's modulus can differ by an average of 3 and 9 GPa for rigid MOFs such as those in the test set. The partial charges calculated by vdW-DF2 deviate the most from other functionals while there is no significant difference between the partial charges calculated by M06L, PBE, PW91, PBE-D2 and PBE-D3 for the MOFs in the test set. We find that while there are differences in the magnitude of the properties predicted by the various functionals, these discrepancies are small compared to the accuracy necessary for most practical applications.

Introduction

Simulations have become an indispensable tool to characterize, screen and design Metal–Organic Frameworks (MOFs).[1–5] The computational methods for molecular adsorption,[1] diffusion,[6,7] and stability[8] in MOFs include classical simulation (Monte Carlo (MC), Molecular Dynamics (MD) or combination MC-MD) as well as plane-wave Density Functional Theory (DFT). The combination of such methods is used in screening procedures to find promising materials for a range of applications.[9–17] The choice of computational methods depends on the size of the system under consideration, the type of property being predicted and the level of accuracy required. For example, classical methods perform well for predicting gas adsorption in materials without strong binding sites but insufficiently describe strong gas/framework interactions.[13,18–21]

There are a large number of options available for each method, including choice of code (LAMMPS,[22] CHARMM,[23] VASP,[24] GAUSSIAN,[25] *etc.*), calculation scheme, parameters (force field choice for classical and functional choice for DFT simulations), *etc.* The choice of an appropriate method is important for the reproduction of material properties. Therefore, the accuracy of and variance within methods should be quantified before application. The performance of a method can be assessed either by comparing its results to the results of a higher-order computational method or the results of a high quality experiment. Higher-order quantum chemical methods such as MP2 (ref. 26) and CCSD(T)[27] have been used to benchmark prediction of structural, thermochemical and electronic properties of small molecules in databases such as the S22 database[28–30] and AM database.[31] These methods can be computationally demanding for property prediction in larger periodic structures. For certain property calculations such as adsorbate/adsorbent binding energies in larger structures like MOFs, it is possible to use fragments to represent the crystal system. However, the size of the fragment can significantly impact the results.[1] Recently, Witte *et al.* have assessed the strengths and weakness of multiple wave-function and DFT methods for gas–ligand interactions in MOFs.[32]

Computational methods used for MOFs are typically assessed by their ability to predict experimental results such as

[a]School of Chemical & Biomolecular Engineering, Georgia Institute of Technology, Atlanta, GA 30332, USA. E-mail: david.sholl@chbe.gatech.edu

[b]Center for Nanophase Materials Sciences, Oak Ridge National Laboratory, Oak Ridge, TN 37831, USA

† Electronic supplementary information (ESI) available: Calculation details, MAD of all calculated structural, elastic and charge properties for each structure and functional. References to original publications for MOFs in test set also included. See DOI: 10.1039/c5ta03864b

lattice parameters and adsorption isotherms. Poloni *et al.* have benchmarked a range of DFT functionals, concluding that vdW-DF and vdW-DF2 approaches can predict CO_2 adsorption enthalpies in MOFs with chemical accuracy.[33] Yu *et al.* have assessed various DFT functionals for prediction of CO_2 adsorption in the CPO-27 MOF by comparing to both experimental and MP2 results.[34] Assessment of the quality of experimental data, specifically structure, for these materials is difficult. However, many computational methods, especially screening procedures, depend critically on access to accurate MOF structure data typically obtained using X-ray powder diffraction (XRPD) or single crystal X-ray diffraction (XRD).[35] These reported structures often include complications such as partially occupied or disordered atoms. A common issue for reported structures is residual solvent left in the MOF pores. Structures reported with residual solvent may have a different structure once solvent is removed. Although there are multiple possible methods to verify the structure of a MOF, including a vast range of quantum chemistry methods,[36] to date there has been no systematic assessment of methods for MOF structure predictions.

The aim of this study is to compile and demonstrate the use of a test set of MOFs with high quality experimental structure data and chemical diversity to assess methods for MOF property predictions. We have benchmarked the performance of DFT functionals for prediction of MOF structure by comparing to the accurate experimental data. We also assess the variance among functionals in DFT prediction of elastic properties and partial charges. Mechanical properties such as Young's modulus, shear modulus, linear compressibility, and Poisson ratio provide MOF flexibility and stability. For example, for MOFs that have a spontaneous ferroelectric polarization, an ease of flexing the materials can result in higher flexoelectricity, a technologically important property that is measurable as well as computable.[37,38] Such properties can be predicted using *ab initio* or classical methods.[39] Although there are no experimental elastic properties available for the structures in the test set we have compiled, we can quantify the variance in predicted values among functionals for a diverse set of MOFs.

Many computational property predictions for MOFs require a description of the electrostatic potential energy surface.[40,41] For classical methods, the electrostatic potential energy surface can be described with point charges assigned to each atom in the structure. These point charges are determined using methods such as the Density Derived Electrostatic and Chemical (DDEC)[42,43] method, which uses *ab initio* derived electron and spin density distributions as input. We studied the impact of DFT functional on the assigned charges by quantifying the variance in assigned charges calculated using a range of functionals for a diverse test set of MOFs.

Methods

Criteria for test set

To ensure high quality structural data, only crystallographic structure information obtained from single crystal X-ray diffraction (XRD) data with an *R*-value of less than 10 was used.

Table 1 Test set of chemically diverse MOFs with high quality experimental crystallographic structure information

Metal	Chemical formula	REFCODE	LCD (Å)
Ag	$Ag_4C_{12}C_{l4}O_8$	RORQOE	1.57
Cd	$Cd_6H_{24}C_{36}N_{36}O_{24}$	GUPCUQ01	12.59
Cd	$Cd_2H_{10}C_{16}N_4O_{10}$	PIJGEV	1.37
Co	$Co_2C_8N_{12}$	HAWVOQ01	1.85
Cu I	$Cu_3H_4C_{10}O_{10}$	MURCEH	3.24
Cu II	$Cu_8H_8C_8N_{12}Cl_8$	QEJZUB01	1.10
Dy	$Dy_2H_{12}C_{12}N_2O_{16}$	YORSII	1.92
Fe	$Fe_4H_4C_4O_{12}$	HOGWAB	1.83
Fe	$Fe_4P_4H_{16}C_8O_{24}$	DEMLIR	1.37
Li, Zn	$Li_{32}Zn_{32}H_{24}C_{72}O_{96}$	WAJJAU	7.48
Sm	$Sm_2H_{12}C_{10}O_{14}$	KOMJEC	3.28
Zn	$Zn_1H_4C_4O_4$	OFUWIV01	1.81

The *R*-value quantifies the agreement of calculated and observed structure factors, with lower *R*-values indicating better structure data.[44] For consistency, only materials with XRD data obtained at room temperature (290–310 K) were considered. XRD data with disorder or residual solvent were excluded. We've chosen to pursue structures that are solvent and disorder free with low *R*-value instead of structures that have been observed frequently in literature. While MOFs like MOF-5, ZIF-8 and HKUST-1 have been widely studied, they are reported with a range of structures, each with slightly different angles and bond lengths. These differences are most likely due to solvent and disorder. We also endeavored to develop a diverse test set as characterized by the metal of the structure building unit (SBU) of each MOF. Twelve different metal centers were chosen, including two different oxidation states of copper and iron. In Table 1, MOFs are denoted using the REFCODE associated with each structure in the Cambridge Structural Database (CSD) and CoRE MOF database.[17]

Benchmarking DFT functional performance for structure predictions

We considered functionals commonly used for MOF structure and property predictions, including the GGA functionals PBE[45,46] and PW91;[47–50] the dispersion corrected functionals PBE-D2,[51] PBE-D3[52,53] and vdW-DF2;[54] and the meta-GGA functional M06L.[55] M06L uses semilocal functionals with parameters fit semiempirically to a diverse data sets which can minimize the deficiencies in treatment of dispersion by traditional functionals.

We chose to include PBE-D3 because unlike PBE-D2, the dispersion coefficient used in PBE-D3 are geometry dependent and are adjusted on the basis of the local coordination number around the atoms of interest. PBE-D3 calculations were carried out using the plane-wave DFT computational package VASP5.3.5. All other calculations were carried out using VASP5.2.12. For all simulations, the Brillouin zone was sampled with a Monkhorst–Pack grid. To determine the parameters for the grid size, two structures were chosen from the test set: a small structure, HAWVOQ01 (Co) with 22 atoms and a moderate

size structure, QEJZUB01 (Cu(I)), with 56 atoms. Each structure was energy minimized with varying grid densities. Based on results shown in Fig. S2,† a grid density of 1000 points per atom was chosen and used for all materials.

The impact of including spin polarization was also studied. Three structures, HAWVOQ01, HOGWAB, and the anti-ferromagnetic DEMLIR with magnetic centers, Co, Fe, and Fe respectively, were chosen from the test set and energy minimized. These structures were analyzed for change in volume, the geometry of the local metal center environment (bond length, bond angle, and torsion angle) and ground state energy. We found that including spin polarization noticeably impacts the volume of all three MOFs (see Fig. S3†). This indicates that spin polarization should be included for some structures with ferromagnetic metals. To determine which structures should include spin polarization, an initial, short DFT calculation was performed for each structure to determine its magnetic moment. Structures found to have high magnetic moments greater than 0.004 μ_B per atom were treated with spin polarization during minimization.

For the two anti-ferromagnetic materials in the test set, DEMLIR (Fe) and MURCEH (Cu), an exhaustive set of initial metal electron spin states were tested. The initial spin configuration that produced the lowest ground state energy was used for remaining calculations. See Table S1† for initial spin states for each metal in the structures.

Simulations were performed in two parts. First, we performed energy minimization for only ionic positions based on a conjugate gradient algorithm. A subsequent minimization used the final positions of the first minimization, introduced the cell shape and volume as degrees of freedom and switched to a quasi-Newton minimization algorithm. For elements with atomic number higher than 94, the missing C_6 and R_0 parameters needed for the PBE-D2 scheme were taken from the D3 scheme (see Table S1†). To determine the performance of the functionals, Cartesian coordinate convergence criteria of a maximum change in system energy of 1×10^{-4} eV per atom and a maximum change in force of 1×10^{-3} eV Å^{-1} were applied to all energy minimization calculations.

The lattice parameters, unit cell volume, bond length, bond angle, and torsion angles associated with the metal center, and pore limiting and largest cavity diameter (PLD and LCD) were measured using the crystallographic data of the experimental and DFT predicted structures. The PLD is defined as the diameter of the largest sphere that can travel along a path throughout the material.[15] The LCD is defined as the largest sphere that can be inserted in the material.[15] These pore diameters were measured using the Zeo++ software.[56–58] For each MOF, the parameters of each predicted structure were compared to those of the experimental structure. Most results are reported in terms of Mean Absolute Deviation (MAD) from the experimental structure parameters, defined as

$$\mathrm{MAD}_f = \sum_i^N \frac{\mathrm{abs}\left(x_{\mathrm{exp},i} - x_i\right)}{N}$$

where f is the functional of interest, N is the total number of bond length, angles, or torsions considered for a MOF or a collection of MOFs, $x_{\mathrm{exp},i}$ is the measured value for the experimental structure and x_i is the measured value for the DFT predicted structure. To determine if the calculated MAD of the five functionals are statistically distinguishable, analysis of variance (ANOVA) tests were applied.

Variance in prediction of mechanical properties

The elastic tensor for each structure was calculated using the strain–stress relationship obtained by six finite distortions of the lattice.[59] All calculations were carried out in VASP. Mechanical properties (Young's modulus, shear modulus, linear compressibility and Poisson's ratio) were calculated using ELATE, a program by Coudert *et al.*[60] The process was repeated for each functional. Convergence tests were performed on 3 of structures with grid densities ranging from 500 to 4000 k points per atom. We found a less than 0.3% difference between moduli calculated for grid densities of 500 and 4000. For consistency with geometry optimization calculations, we chose 1000 points per atom grid density.

DDEC point charges

Charges were assigned using the January 2014 version of the Density Derived Electrostatic and Chemical (DDEC) program provided by Manz *et al.*[42] DDEC charges have been tested for dense and porous solids, surfaces of solids, small molecules, and large molecules with buried atoms.[61] The electron and spin density distributions used as input for the DDEC code were generated with VASP. Single ionic step self-consistent plane wave DFT calculations with each functional were performed using the same criteria described for energy minimization of the test set. Given that Grimme dispersion corrections are added after the DFT calculation, PBE-D2 and PBE-D3 calculations will result in the same charge density as PBE after a single step. Therefore, D2 and D3 were not included in these calculations. While the DDEC method provides an individual charge for each atom in the system, it is computationally more convenient to distinguish between atom types within a structure. Therefore, point charges were assigned for each atom type in a structure. Atom types are assigned based on the atom's neighboring environment and charges for each atom type are averaged to obtain a net neutral system.

Results

An initial set of candidate materials was chosen from the CoRE MOF database.[17] Of the thousands of already synthesized MOFs, approximately 2000 structures were found to be solvent and disorder free. Three quarters of these structures were porous but only 300 qualified as high quality based on R-value. The 300 structures consisted of 75 different metal types, including MOFs with multiple metals. Of these, twelve structures, with a different metal center including two oxidation states of copper and iron (commonly found in MOFs), were chosen for the test set. To increase topological porosity, we included an additional cadmium MOF with a large LCD of 12.59 Å. As shown in Table 1, structures also vary in porosity with a LCD range of 1.1–12.6 Å.

Benchmarking of DFT functionals for prediction of MOF structure

To compare the performance for overall structure prediction, the predicted lattice parameters and volume of each structure were compared to the experimental values. Fig. 1 shows the MAD and the corresponding 95% confidence interval, indicated by error bars, of all lattice parameters and volumes in the test set.

Fig. 1(b) shows an up to 8% MAD in volume for the structures in the test set. Simulations of properties such as gas adsorption typically require that lattice parameters be accurate within a few percent. The larger change in volume seen in Fig. 1(b) are primarily due to the small size of the unit cells in the test set. In such small structures, minor changes in the lattice parameters result in relatively large percent change in cell volume. While there is a difference in the MAD of lattice parameters among the functionals, the MAD of less than 0.3 Å is insignificant relative to the accuracy necessary for most applications.

The dashed lines in Fig. 1 show that there is essentially no overlap of the confidence intervals of PBE-D2 and PBE-D3 with PBE, PW91, M06L or vdW-DF2. That is, the MAD of PBE-D2 and D3 predicted lattice parameters and volumes show a statistically significant difference from PBE, PW91, and M06L functional predicted values.

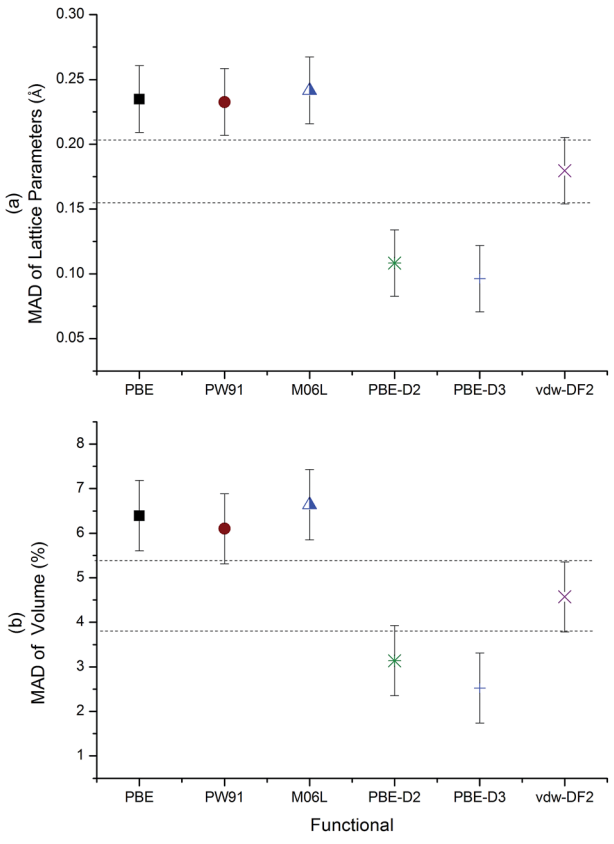

Fig. 1 The MAD and the corresponding 95% confidence interval (shown as error bars) of all predicted (a) lattice parameters and (b) unit cell volume relative to the experimental structure. The dashed lines encompassing the 95% confidence interval of the vdW-DF2 MAD overlap with values of all other functionals.

The unit cell volumes for the individual materials in the test set are shown in Fig. 2. The dispersion corrected functionals, PBE-D2, PBE-D3 and vdW-DF2, are in general closest to the experimental values and tend to underpredict unit cell volumes. It is important to note that no single functional is the most accurate for all materials. Examples exist, for instance, where the dispersion corrected functionals do not give the most accurate results.

The RORQOE (Ag) DFT predicted structure with PBE, shown in Fig. 3, has the largest deviation in unit cell parameters (0.5 Å, 0.3 Å, 1.0 Å), shape (orthorhombic to triclinic) and volume (12%). This is due largely to the 10 degrees overprediction of an O–Ag–Cl angle by the PBE, PW91, and M06L functionals. This particular bond angle is predicted more accurately by the PBE-D2 and vdW-DF2 functionals, with a deviation of less than 0.5°. Fig. S4† examines this example in terms of the charge density predictions of representative functionals.

Deviations from experimentally predicted structures were investigated in more detail through analysis of bonded interactions. Only bond lengths associated with the metal center and bond and torsion angles with a metal at the center were considered. As shown in Fig. 4, when averaged among all structures, torsion angles predicted with vdW-DF2 deviate the least from the experimental structures. The MAD of bond angles show that PBE-D3 predicted bond angles deviate the least on average from experimentally observed bond angles.

The dashed lines in Fig. 4(b) show that the confidence interval of vdW-DF2 MAD for bond angles overlaps with the MAD interval of the PBE-D2 functional. However, the average deviations in bonded interactions are small relative to the accuracy necessary for most applications. When the performance of the different functionals was compared for each structure, we found that the largest deviation in bond length, 0.25 Å is seen in a Cu–N bond of QEJZUB01 predicted by PBE.

The absolute deviation for the predicted bond angles within a MOF were averaged for each MOF in the test set. No MOFs were found with significant differences among the MAD of PBE,

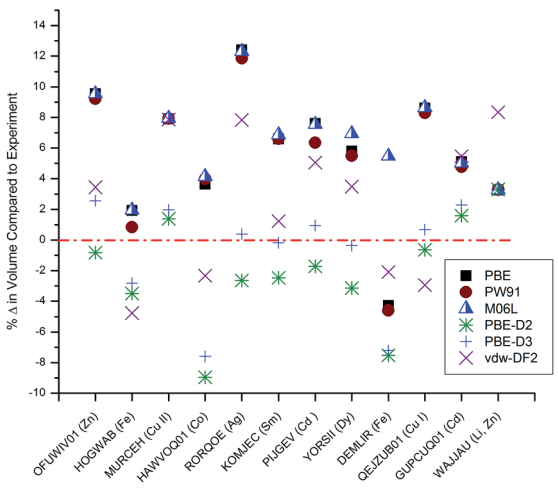

Fig. 2 The percent deviation of unit cell volume from the experimental structure for each material in the test set. Structures ordered with increasing unit cell volume.

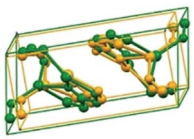

Fig. 3 The RORQOE (Ag) structure, with yellow representing the experimental structure and green represents the PBE predicted structure, shows a change in shape and size of the unit cell.

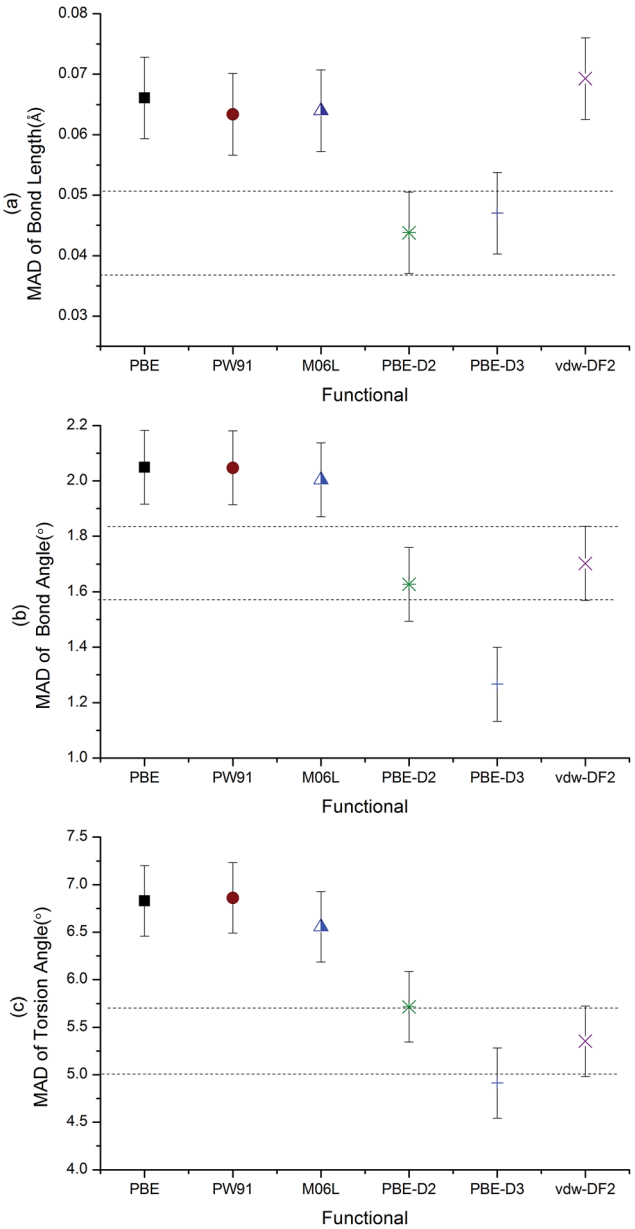

Fig. 4 The MAD and the 95% confidence interval of bonded parameters relative to the experimental structure are shown. (a) MAD of bond lengths (b) MAD of bond angles (c) MAD of torsion angles.

PW91 and M06L predicted bond angles. In the twelve structures, only nine structures were found to have a statistically significant difference in bond angle prediction among functionals. The PBE-D2 and vdW-DF2 predicted a lower deviation for four structures, while PBE, PW91 and M06L predict a lower deviation for three structures.

We observed large deviations of specific angles in the RORQOE (Ag) and HOGWAB (Fe) structures. As discussed earlier, PBE, PW91, and M06L predicted RORQOE (Ag) O–Ag–Cl angles deviate by 12° while vdW-DF2 and PBE-D2 predict the angles more accurately; see Table S8† for the type and magnitude of angles considered. For HOGWAB (Fe II), some vdW-DF2 and PBE-D2 predicted O–Fe–O angles deviate by 13° while PBE, PW91 and M06L functionals predict the angles more accurately. This supports the concept that there is no "one size fits all" option for functionals in terms of accurately predicting MOF structures. This observation suggests that selecting a functional to optimize MOF structures based largely on computational accessibility or efficiency is a reasonable approach.

Torsion angles are typically softer degrees of freedom than bond angles and can have larger deviations without significant impact on the structure. In our study we observed deviations in the range of 0.5–20° for torsion angles. When comparing the MAD of torsion angles for structures individually, vdW-DF2 or PBE-D2 results in the lowest MAD for only five structures. One such example is HAWVOQ01 (Co), with a more than 7° degree larger MAD for PW91 than PBE-D2 (see Table S5†). These differences in torsion angle are apparent in the shift in pore morphology as show in Fig. 5. PBE, PW91 and M06L outperformed PBE-D2 and vdW-DF2 with statistical significance for only two structures, DEMLIR and HOGWAB. We found that the HOGWAB iron MOF (with spin polarization included in the DFT predictions) showed a larger deviation between DFT predicted and experimentally observed structures.

Despite deviations in torsion angles, the deviations from the calculated PLD and LCD of the experimental crystallographic structure data are less than 0.5 Å. One-way ANOVA analysis of the deviation of PLDs and LCDs from the experimental values show there is no statistical difference between the MAD of pore descriptors calculated by any of the functionals. That is, we have no evidence that any functional performs better than another (see S4†). When considering the mean deviation of PLDs and LCDS, we find that PBE-D2 and vdW-DF2 tend to underpredict PLDs (see Tables S6 and S7†).

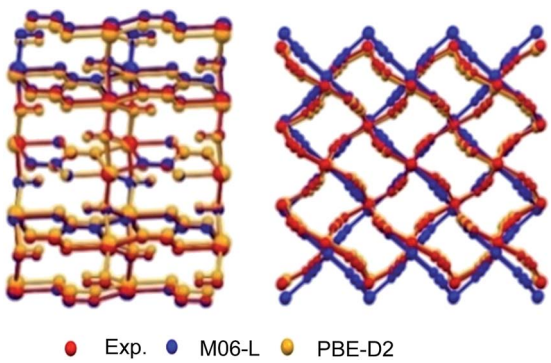

Fig. 5 Impact of large deviation in torsion angle on pore morphology on HOGWAB (Fe II) and HAWVOQ01 (Co).

Mechanical properties

The minimum and maximum Young's modulus, shear modulus, linear compressibility and Poisson ratio were calculated for all twelve structures. Fig. 6(a) shows the minimum Young's modulus for 10 of 12 structures in the test set, calculated with PBE, PW91, M06L, vdW-DF2, PBE-D2, and PBE-D3 functionals. The results show that the test set includes a wide range of Young's modulus in the MOF's direction of lowest rigidity. According to the nomenclature of Ortiz *et al.*, the large values for minimum Young's modulus indicate that the test set does not contain flexible materials.[39] Fig. 6(b) shows similar trends for the minimum shear modulus of the test set MOFs.

When comparing results among functionals, we find that on average vdW-DF2 predicts a more rigid structure. In rigid structures, the minimum Young's modulus has a standard deviation of 9 GPa among functionals and shear a standard deviation of 3 GPa. For some structures, results can differ up to 20 GPa. While this provides a clear distinction between functionals, a 20 GPa deviation is not large relative to the typical accuracy of experimental results available for elastic properties of rigid MOFs such as those in the test set. Tan *et al.* found that calculated values for moduli are noticeably higher than experimental observations, potentially due to physical degradation of the crystals.[62]

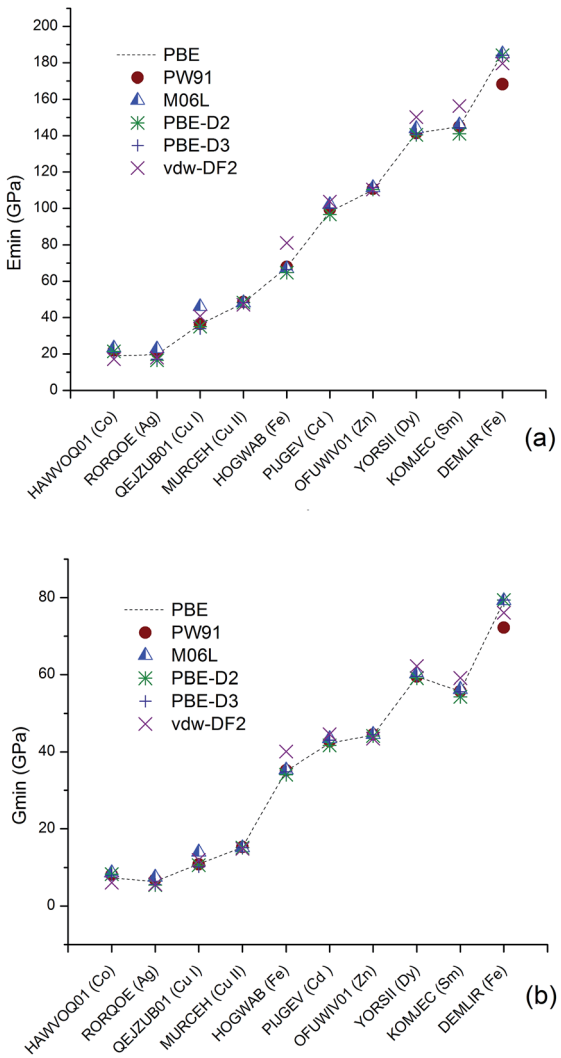

Fig. 6 The predicted magnitude of the (a) Young's modulus and (b) shear modulus in the direction of least rigidity for each structure computed using six functionals. Results with PBE are shown with a dotted line to guide the eye.

As shown in Fig. 6, the minimum Young's modulus calculated by M06L for QEJZUB01 (Cu I) noticeably deviates from PBE and PW91. Similarly, M06L calculated maximum linear compressibility and Poisson ratio also deviate significantly, up to 20%, from PBE calculated values. This deviation is higher than those observed for other structures in the test set. The direction of minimum Young's modulus for QEJZUB01 is along the channel axis of the *yz* plane, see Fig. 7. Two of the four sides of this channel are dominated by Cl–Cu–Cl bonds. Deformations in these bonds are also responsible for the maximum linear compressibility. Similarly, the Cl–Cu–N bonds adjacent to the channels of the MOF are the primary bonds under strain in the direction of the maximum Poisson ratio of QEJZUB01.

We find similar deviations of M06 from PBE calculated elastic properties for RORQOE (Ag), another Cl containing MOF. RORQOE has oval shaped channels that run diagonally across its unit cell. The Young's modulus, maximum linear compressibility and Poisson ratio of RORQOE are all properties related to distortions associated with torsion angles of Cl–Ag–O–Ag. For these properties, M06 predict an approximately 20% more rigid MOF than PBE calculated values.

Because of the absence of experimental data, we cannot conclude which functional accurately predicts the elastic properties of these MOFs. However, results for our test set show that vdW-DF2 on average predicts higher rigidity for MOFs compared to other functionals. We also find that while M06 produces comparable results to PBE and PW91 for most MOFs, it predicts more rigid properties associated with Cl–metal bonds. However, the magnitude of the differences among the functionals is small relative to the precision of experimental results.

Partial charges

Partial charges on individual atoms are not experimental observables, but they are crucial ingredients in many atomistic simulation methods. We examined the influence of functionals on the assignment of partial charges in two ways. First, we considered differences in partial charges between calculations with different functionals. Second, for each functional, we examined the change in partial charges between calculations using the experimentally observed MOF structure and DFT optimized structure.

To compare predicted atomic charges using different functionals, we calculated the DDEC partial charges for only the experimental structure of the MOFs in the test set based on the charge density calculated by PBE, PW91, M06L and vdW-DF2. For each MOF, atoms with similar charge and same coordination were categorized into atom types, resulting in 100 atom types. To quantify the variance in assigned changed among

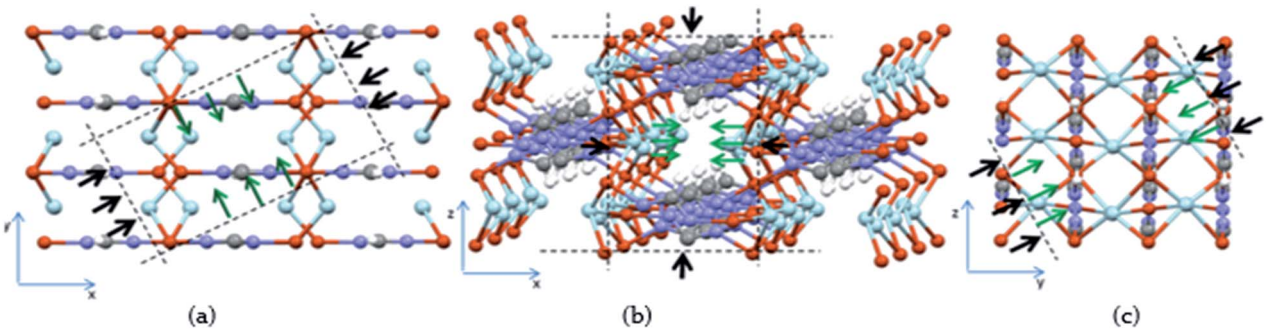

Fig. 7 The structure of QEJZUB01 (Cu I) with black arrows showing direction of stress and green arrows showing direction of strain in (a) maximum Poisson ratio, (b) maximum linear compressibility, and (c) minimum Young's modulus.

functionals, we calculated the mean absolute deviation relative to other functionals. The MAD for charges is defined as

$$\mathrm{MAD}_f = \sum_i \sum_{j \neq f} \frac{\left(x_i^f - x_i^j\right)}{3N}$$

where f is the functional of interest, i is atom type, j is all functionals other than f, x is the DDEC charge, and N is the number of atom types.

One-way ANOVA analysis of the arc cosine normalized partial charges show no difference between the MAD of partial charges calculated by PBE, PW91, and M06L for the MOFs in our test set (see Table 2). Unlike the MAD calculated for structural parameters, the magnitude of the MAD calculated for changes here only captures if there is a statistically difference between the predicted charges by different functionals and does not represent the average deviation from a value calculated for an experimental structure. Overall, the variation in partial charges between calculations with different functionals is small. This is consistent with the earlier results of Manz *et al.* for DFT calculations with a range of materials.[61]

Partial charges calculated by vdW-DF2 deviate the most from the calculations of other functionals. The largest deviation was 0.12 electrons for phosphorus in DEMLIR (Fe II) where vdW-DF2 predicted larger charge transfer. Previous studies suggest that the self-consistent vdW-DF2 method is most accurate for layered materials with magnetic metal ions where the charge-transfer plays a crucial role in predicting the spin-polarized electronic configuration of the ion and modifies its polarizability significantly compared to the metal-atom and hence equivalently the empirical C_6 parameter in the Grimme parametrization.[63]

Table 2 The MAD and the 95% confidence interval of partial charges

	MAD	Confidence interval (±)
PBE	0.0359	0.0042
PW91	0.0380	0.0042
M06L	0.0357	0.0042
vdW-DF2	0.0961	0.0042

To test the impact of charge transfer as described by vdW-DF2 on prediction of MOF structure, we compared the MAD of predicted partial charges to the difference in MAD of vdW-DF2 and PBE-D2 for structural parameters (see Table S16†). However, no correlation was found between larger charge transfer being predicted by vdW-DF2 and better prediction of structural parameters when compared to PBE-D2.

As discussed above, optimization of MOF structures with DFT gives structures that deviate slightly from experimentally observed crystal structures. To assess the impact of these deviations on partial charges, we calculated the partial charges of the DFT energy minimized structures and compared them to charges calculated for the experimental structure.

For simplicity, we used PBE to assign the partial charges in all cases, noting from the discussion above that the variation in partial charges among functionals (for the same structure) is small. Fig. 8 shows the MAD of PBE partial charges for each DFT predicted structure relative to the experimental structure. On average, partial charges change by less than 0.06 electrons.

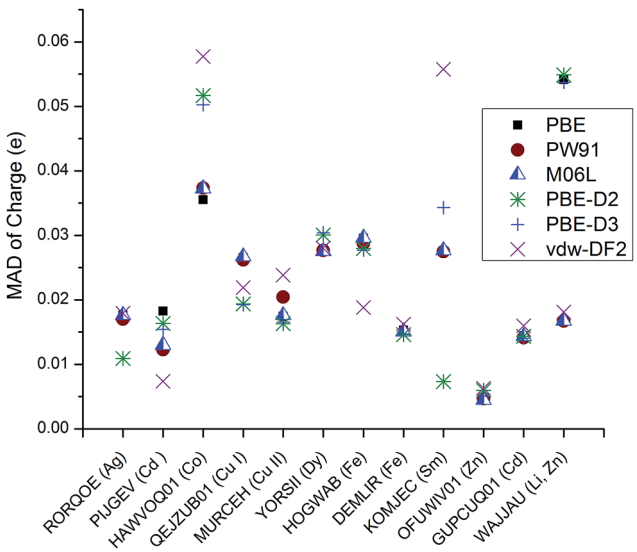

Fig. 8 The MAD of partial charges calculated for DFT minimized structures (minimized using PBE, PW91, M06L, PBE-D2, PBE-D3, and vdW-DF2) from the partial charges calculated the experimental structures. All partial charges calculated with PBE functional.

The oxygen atom connected to a Sm atom in the vdW-DF2 predicted KOMJEC (Sm) has the largest change in charge of 0.3 electrons. These results suggest that assigning partial charges directly from experimentally observed MOF structures is likely to be sufficient to provide accurate charges for atomistic simulations; the additional effort of optimizing a structure using DFT prior to assigning charges leads to little change in the assigned charges.

Conclusions

We have compiled a test set of chemically diverse MOFs with high accuracy experimentally derived crystallographic structure data. The test set contains MOFs with a range of topologies and elastic properties. We have demonstrated the significance of a test set with high accuracy structural data by benchmarking the performance of DFT functionals for predicting lattice parameters, unit cell volume, bonded parameters and pore descriptors. For MOFs with magnetic metals, spin polarization can significantly impact structure prediction. We have found that on average PBE-D2, PBE-D3, and vdW-DF2 calculations predict a lower deviation in structure than the other functionals we tested. However, we found that M06L, PBE, and PW91 each predict lower deviation for some MOFs in the test set. Despite deviations in unit cell and bonded parameters, we found that all functionals predicted the PLD and LCD for every MOF in the test set within 0.5 Å of the experimental value.

We have also demonstrated the significance of a chemically diverse test set by assessing the variance in DFT functional performance for properties where accurate experimental values are unavailable. We first showed that DFT predicted elastic properties such as the minimum shear modulus and Young's modulus can differ by an average of 3 and 9 GPa for rigid MOFs such as those in the test set. This deviation is small relative to the precision of experimental results available for elastic properties of MOFs. By calculating DDEC partial charges, we found that there is no correlation between the DFT functional's ability to reproduce structural parameters and electrostatic potential surface of a MOF. When assessing the variance in assigned changed among functionals, we showed that there is no difference between the MAD of partial charges calculated by PBE, PW91, and M06L for the MOFs in our test.

Our results indicate that there is no "one size fits all" functional suitable for accurately predicting the structure and other properties of MOFs. That is, no single functional shows accuracy that demonstrates strong statistical significance over other functionals for the full range of MOFs in our test set. Although the choice of specific functional may be justified in some limited instances, it appears that the choice of functional for efforts aimed at screening large numbers of MOFs can justifiably be made based on computational convenience and availability.

Acknowledgements

This work was supported by the Nanoporous Materials Genome Center. This research benefitted from computing resources at the Center for Nanophase Materials Sciences, which is a DOE Office of Science User Facility and used resources of the National Energy Research Scientific Computing Center, a DOE Office of Science User Facility supported by the Office of Science of the U.S. Department of Energy under Contract No. DE-AC02-05CH11231. We thank Prof. Thomas Manz for assistance with code for computing DDEC charges.

Notes and references

1 R. B. Getman, Y. S. Bae, C. E. Wilmer and R. Q. Snurr, *Chem. Rev.*, 2012, **112**, 703–723.
2 T. Duren, Y. Bae and R. Snurr, *Chem. Soc. Rev.*, 2009, **38**, 1237–1247.
3 J. W. Jiang, *Mol. Simul.*, 2014, **40**, 516–536.
4 S. S. Han, J. L. Mendoza-Cortes and W. A. Goddard, *Chem. Soc. Rev.*, 2009, **38**, 1460–1476.
5 S. Keskin, J. Liu, R. B. Rankin, J. K. Johnson and D. S. Sholl, *Ind. Eng. Chem. Res.*, 2009, **48**, 2355–2371.
6 A. I. Skoulidas and D. S. Sholl, *J. Phys. Chem. B*, 2005, **109**, 15760–15768.
7 J. Li, R. Kuppler and H. Zhou, *Chem. Soc. Rev.*, 2009, **38**, 1477–1504.
8 Y. Cai, A. R. Kulkarni, Y. G. Huang, D. S. Sholl and K. S. Walton, *Cryst. Growth Des.*, 2014, **14**, 6122–6128.
9 Y. J. Colon and R. Q. Snurr, *Chem. Soc. Rev.*, 2014, **43**, 5735–5749.
10 S. G. Han, Y. G. Huang, T. Watanabe, Y. Dai, K. S. Walton, S. Nair, D. S. Sholl and J. C. Meredith, *ACS Comb. Sci.*, 2012, **14**, 263–267.
11 J. Jelic, D. Denysenko, D. Volkmer and K. Reuter, *New J. Phys.*, 2013, **15**, 115004–115015.
12 C. E. Wilmer, M. Leaf, C. Y. Lee, O. K. Farha, B. G. Hauser, J. T. Hupp and R. Q. Snurr, *Nat. Chem.*, 2012, **4**, 83–89.
13 A. O. Yazaydin, R. Q. Snurr, T. H. Park, K. Koh, J. Liu, M. D. LeVan, A. I. Benin, P. Jakubczak, M. Lanuza, D. B. Galloway, J. J. Low and R. R. Willis, *J. Am. Chem. Soc.*, 2009, **131**, 18198–18199.
14 C. E. Wilmer and R. Q. Snurr, *Chem. Eng. J.*, 2011, **171**, 775–781.
15 E. Haldoupis, S. Nair and D. Sholl, *J. Am. Chem. Soc.*, 2010, **132**, 7528–7539.
16 T. Watanabe, S. Keskin, S. Nair and D. S. Sholl, *Phys. Chem. Chem. Phys.*, 2009, **11**, 11389–11394.
17 Y. G. Chung, J. Camp, M. Haranczyk, B. J. Sikora, W. Bury, V. Krungleviciute, T. Yildirim, O. K. Farha, D. S. Sholl and R. Q. Snurr, *Chem. Mater.*, 2014, **26**, 6185–6192.
18 A. L. Dzubak, L. C. Lin, J. Kim, J. A. Swisher, R. Poloni, S. N. Maximoff, B. Smit and L. Gagliardi, *Nat. Chem.*, 2012, **4**, 810–816.
19 L. Chen, C. Morrison and T. Duren, *J. Phys. Chem. C*, 2012, **116**, 18899–18909.
20 M. Fischer, J. Gomes, M. Froba and M. Jorge, *Langmuir*, 2012, **28**, 8537–8549.
21 M. Fischer, B. Kuchta, L. Firlej, F. Hoffman and M. Froba, *J. Phys. Chem. C*, 2010, **114**, 19116–19126.
22 S. Plimpton, *J. Comput. Phys.*, 1995, **117**, 1–19.

23 B. R. Brooks, R. E. Bruccoleri, B. D. Olafson, D. J. States, S. Swaminathan and M. Karplus, *J. Comput. Chem.*, 1983, **4**, 187–217.
24 G. Kresse and J. Furthmuller, *Phys. Rev. B: Condens. Matter Mater. Phys.*, 1996, **54**, 11169–11186.
25 M. J. Frisch, G. W. Trucks, H. B. Schlegel, G. E. Scuseria, M. A. Robb, J. R. Cheeseman, G. Scalmani, V. Barone, B. Mennucci, G. A. Petersson, H. Nakatsuji, M. Caricato, X. Li, H. P. Hratchian, A. F. Izmaylov, J. Bloino, G. Zheng, J. L. Sonnenberg, M. Hada, M. Ehara, K. Toyota, R. Fukuda, J. Hasegawa, M. Ishida, T. Nakajima, Y. Honda, O. Kitao, H. Nakai, T. Vreven, J. A. Montgomery Jr, J. E. Peralta, F. Ogliaro, M. J. Bearpark, J. Heyd, E. N. Brothers, K. N. Kudin, V. N. Staroverov, R. Kobayashi, J. Normand, K. Raghavachari, A. P. Rendell, J. C. Burant, S. S. Iyengar, J. Tomasi, M. Cossi, N. Rega, N. J. Millam, M. Klene, J. E. Knox, J. B. Cross, V. Bakken, C. Adamo, J. Jaramillo, R. Gomperts, R. E. Stratmann, O. Yazyev, A. J. Austin, R. Cammi, C. Pomelli, J. W. Ochterski, R. L. Martin, K. Morokuma, V. G. Zakrzewski, G. A. Voth, P. Salvador, J. J. Dannenberg, S. Dapprich, A. D. Daniels, Ö. Farkas, J. B. Foresman, J. V. Ortiz, J. Cioslowski and D. J. Fox, Gaussian, Inc. Wallingford CT, *Gaussian 09*, 2009.
26 C. Moller and M. S. Plesset, *Phys. Rev.*, 1934, **46**, 0618–0622.
27 M. Musial and R. J. Bartlett, *J. Chem. Phys.*, 2007, **127**, 024106.
28 P. Jurecka, J. Sponer, J. Cerny and P. Hobza, *Phys. Chem. Chem. Phys.*, 2006, **8**, 1985–1993.
29 Y. Zhao and D. G. Truhlar, *J. Phys. Chem. C*, 2008, **112**, 4061–4067.
30 Y. Zhao and D. G. Truhlar, *Acc. Chem. Res.*, 2008, **41**, 157–167.
31 M. Korth and S. Grimme, *J. Chem. Theory Comput.*, 2009, **5**, 993–1003.
32 J. Witte, J. Neaton and M. Head-Gordon, *J. Chem. Phys.*, 2014, **140**, 104707.
33 R. Poloni, B. Smit and J. Neaton, *J. Phys. Chem. A*, 2012, **116**, 4957–4964.
34 D. Yu, A. Yazaydin, J. Lane, P. Dietzel and R. Snurr, *Chem. Sci.*, 2013, **4**, 3544–3556.
35 P. A. Jacobs, E. M. Flanigen, J. C. Jansen and H. van Bekkum, *Introduction to Zeolite Science and Practice*, Elsevier Science, 2001.
36 S. Odoh, C. Cramer, D. Truhlar and L. Gagliardi, *Chem. Rev.*, 2015, **115**, 6051–6111.
37 W. Zhang and R. G. Xiong, *Chem. Rev.*, 2012, **112**, 1163–1195.
38 J. W. Hong and D. Vanderbilt, *Phys. Rev. B: Condens. Matter Mater. Phys.*, 2013, **88**, 174107.
39 A. U. Ortiz, A. Boutin, A. H. Fuchs and F. X. Coudert, *Phys. Rev. Lett.*, 2012, **109**, 195502.
40 J. R. Karra and K. S. Walton, *Langmuir*, 2008, **24**, 8620–8626.
41 Q. Y. Yang and C. L. Zhong, *ChemPhysChem*, 2006, **7**, 1417–1421.
42 T. A. Manz and D. S. Sholl, *J. Chem. Theory Comput.*, 2012, **8**, 2844–2867.
43 T. Watanabe, T. A. Manz and D. S. Sholl, *J. Phys. Chem. C*, 2011, **115**, 4824–4836.
44 P. Jones, *Chem. Soc. Rev.*, 1984, **13**, 157–172.
45 J. P. Perdew, K. Burke and Y. Wang, *Phys. Rev. B: Condens. Matter Mater. Phys.*, 1996, **54**, 16533–16539.
46 J. P. Perdew, K. Burke and M. Ernzerhof, *Phys. Rev. Lett.*, 1997, **78**, 1396.
47 J. P. Perdew, J. A. Chevary, S. H. Vosko, K. A. Jackson, M. R. Pederson, D. J. Singh and C. Fiolhais, *Phys. Rev. B: Condens. Matter Mater. Phys.*, 1993, **48**, 4978.
48 J. P. Perdew, J. A. Chevary, S. H. Vosko, K. A. Jackson, M. R. Pederson, D. J. Singh and C. Fiolhais, *Phys. Rev. B: Condens. Matter Mater. Phys.*, 1992, **46**, 6671–6687.
49 J. P. Perdew, K. Burke and Y. Wang, *Phys. Rev. B: Condens. Matter Mater. Phys.*, 1998, **57**, 14999.
50 J. P. Perdew, K. Burke and M. Ernzerhof, *Phys. Rev. Lett.*, 1996, **77**, 3865–3868.
51 S. Grimme, *J. Comput. Chem.*, 2006, **27**, 1787–1799.
52 S. Grimme, J. Antony, S. Ehrlich and H. Krieg, *J. Chem. Phys.*, 2010, **132**, 154104.
53 S. Grimme, S. Ehrlich and L. Goerigk, *J. Comput. Chem.*, 2011, **32**, 1456–1465.
54 K. Lee, E. D. Murray, L. Z. Kong, B. I. Lundqvist and D. C. Langreth, *Phys. Rev. B: Condens. Matter Mater. Phys.*, 2010, **82**, 081101.
55 Y. Zhao and D. G. Truhlar, *J. Chem. Phys.*, 2006, **125**, 194101.
56 R. L. Martin, B. Smit and M. Haranczyk, *J. Chem. Inf. Model.*, 2012, **52**, 308–318.
57 T. F. Willems, C. Rycroft, M. Kazi, J. C. Meza and M. Haranczyk, *Microporous Mesoporous Mater.*, 2012, **149**, 134–141.
58 M. Pinheiro, R. L. Martin, C. H. Rycroft, A. Jones, E. Iglesia and M. Haranczyk, *J. Mol. Graphics Modell.*, 2013, **44**, 208–219.
59 Y. le Page and P. Saxe, *Phys. Rev. B: Condens. Matter Mater. Phys.*, 2002, **65**, 104104.
60 A. U. Ortiz, A. Boutin, A. H. Fuchs and F. X. Coudert, *J. Chem. Phys.*, 2013, **138**, 174703.
61 T. A. Manz and D. S. Sholl, *J. Chem. Theory Comput.*, 2010, **6**, 2455–2468.
62 J. C. Tan and A. K. Cheetham, *Chem. Soc. Rev.*, 2011, **40**, 1059–1080.
63 P. Ganesh, J. Kim, C. Park, M. Yoon, F. A. Reboredo and P. R. C. Kent, *J. Chem. Theory Comput.*, 2014, **10**, 5318–5323.

